Three-body recombination in cold helium–helium–alkali-metal-atom collisions

Hiroya Suno
The Earth Simulator Center, Japan Agency for Marine-Earth Science and Technology, 3173-25 Showa-machi, Kanazawa-ku, Yokohama 236-0001, Japan

B. D. Esry
Department of Physics, Kansas State University, Manhattan, Kansas 66506, USA
(Received 19 June 2009; published 2 December 2009)

Three-body recombination in helium-helium–alkali-metal collisions at cold temperatures is studied using the adiabatic hyperspherical representation. The rates for the three-body recombination processes $^4\mathrm{He}+^4\mathrm{He}+X \rightarrow ^4\mathrm{He}+^4\mathrm{He}X$ and $^4\mathrm{He}+^4\mathrm{He}+X \rightarrow ^4\mathrm{He}_2+X$, with $X=^7\mathrm{Li}$, $^{23}\mathrm{Na}$, $^{39}\mathrm{K}$, $^{85}\mathrm{Rb}$, and $^{133}\mathrm{Cs}$, are calculated at nonzero collision energies by including not only zero total angular momentum, $J=0$, states but also $J>0$ states. The three-body recombination rates show a relatively weak dependence on the alkali-metal species, differing from each other only by about one order of magnitude, except for the ^{4}He-^{4}He-^{23}Na system.

DOI: 10.1103/PhysRevA.80.062702 PACS number(s): 34.10.+x, 34.50.−s

I. INTRODUCTION

Three-body recombination is a three-particle process in which two particles form a bound state and the third one carries away the binding energy. This process has attracted much interest since it is one of the most important loss mechanisms for trapped ultracold atoms. It is also important in nuclear physics and in the chemical dynamics of combustion and gas-phase systems. Several experiments have been carried out on ultracold atomic gases, emphasizing the importance of three-body recombination to determining the lifetime and stability of these gases [1–3]. One of the most remarkable tools in these investigations is the use of external magnetic fields near a Feshbach resonance to control the atomic interactions, which is characterized by the two-body s-wave scattering length a. It is also through the measurement of three-body recombination rates, exploiting a Feshbach resonance in an ultracold gas of ^{133}Cs atoms [4], that evidence of Efimov physics [5–7] was experimentally seen for the first time.

On the theoretical side, there have also been numerous studies of three-body recombination in the past decade. Most of these investigations use model interaction potentials, based on the assumption that the three-body recombination rates in the ultracold limit depend solely on the two-body scattering length a, but not on the precise shape of the two-body interaction potential. From earlier studies, the recombination rate of three identical bosons was predicted [8–11] (and verified experimentally [3]) to increase with the scattering length as a^4. More recently, a review summarizing the developments in analytical treatments of zero-temperature recombination has appeared [12]. D'Incao and Esry [13] presented both the energy and scattering length dependence of the three-body recombination rate as well as those of the vibrational relaxation and collision-induced dissociation rates for systems including three identical bosons, two identical bosons, and two identical fermions.

Thus far, however, besides the Ne-Ne-H system studied by Parker *et al.* [14], triatomic helium systems are the only realistic systems that have been treated fully quantum mechanically in the studies of ultracold three-body recombination. The treatment of triatomic ^{4}He systems is simple compared to other atomic species because there exists only one dimer bound state that has zero orbital angular momentum $l=0$. The large numbers of atom-molecule channels present for other realistic systems currently pose difficulties for theoretical treatments. Several sophisticated helium dimer interaction potentials have been developed, such as the LM2M2 potential by Aziz and Slaman [15], and the HFD-B3-FCI1 potential by Aziz *et al.* [16]. The latter potential has been used to calculate the three-body recombination rates of ^{4}He atoms [17–19]. Kolganova *et al.* [20] used the LM2M2 and other potentials to study ultracold collisions of ^{3,4}He atoms with $^4\mathrm{He}_2$ dimers. Jeziorska *et al.* [21] and Cencek *et al.* [22] recently developed not only a helium dimer potential, but also the retardation corrections and the nonadditive three-body term, which we adopted in our previous work [23] to calculate the rates for the recombination processes $^4\mathrm{He}+^4\mathrm{He}+^{3,4}\mathrm{He} \rightarrow ^4\mathrm{He}_2+^{3,4}\mathrm{He}$, as well as the collision-induced dissociation rates.

In addition to the well-studied triatomic helium systems, there exist other examples of triatomic systems that have only a small number of atom-molecule channels. The interaction potentials between He and alkali-metal atoms, for instance, have very shallow wells. These potentials have been investigated since the 1970s by Dehmer and Wharton [24] from scattering experiments. Theoretically, the interaction potentials for the helium–alkali-metal systems have been obtained by Kleinekathöfer [25,26]. It turns out that the He–alkali-metal potentials are even weaker than the He-He potential (see Fig. 1) and the ^{4}He–alkali-metal systems support only one bound state with zero orbital angular momentum $l=0$, as well, whereas among the ^{3}He–alkali-metal systems only ^{3}He-^{23}Na has one bound state with $l=0$. Therefore, it follows that for the helium-helium–alkali-metal (^{4}He-^{4}He-X) systems there exist only two atom-molecule channels: one corresponding to $^4\mathrm{He}+^4\mathrm{He}X$ and the other to $^4\mathrm{He}_2+X$.

In this paper, we study three-body recombination for cold helium-helium–alkali-metal systems. This work extends the previous investigations in Refs. [17–19,23], which dealt with

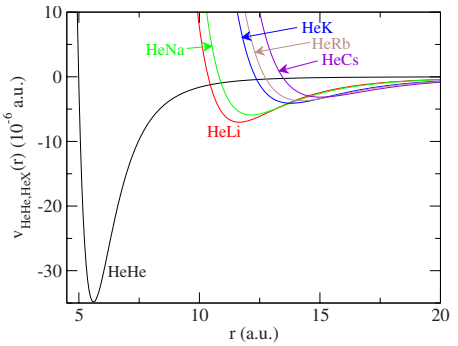

FIG. 1. (Color online) Helium dimer potential curve $v_{\mathrm{HeHe}}(r)$ taken from Ref. [21]. and helium–alkali-metal $v_{\mathrm{He}X}(r)$ potential curves from Ref. [26].

cold three-body recombination of helium triatomic systems. Such a collision process is important in ultracold gas experiments using buffer-gas cooling, since it might limit the lifetimes of the trapped atoms. The theoretical treatment of ^{4}He-^{4}He-X systems is still relatively simple since there exist only two atom-molecule channels, as mentioned above. We calculate the rates for the three-body recombination processes $^4\mathrm{He}+{}^4\mathrm{He}+X\rightarrow{}^4\mathrm{He}_2+X$ and $^4\mathrm{He}+{}^4\mathrm{He}+X\rightarrow{}^4\mathrm{He}+{}^4\mathrm{He}X$ at finite temperatures, taking into account not only zero total orbital angular momentum, $J=0$, states but also $J>0$ states. As far as we know, this is the first time that three-body recombination for these systems has been studied. We adopt the He-He dimer interaction potential by Jeziorska *et al.* [21] and the Kleinekathöfer-Tang-Toennies-Yiu (KTTY) helium–alkali-metal potential by Kleinekathöfer *et al.* [26].

The key ingredient in our numerical calculations is the adiabatic hyperspherical representation [17,27,28]. A modified version of the Smith-Whitten coordinate system [17,23,29,30] is combined with specific boundary conditions to impose the permutation symmetry of the two bosonic ^{4}He atoms. The R-matrix method [31,32] is then used to obtain the scattering S matrix, which allows us to calculate the three-body recombination rates K_3. Note that the rate equation for the density of helium atoms in a thermal gas can be written as

$$\frac{dn_{\mathrm{He}}}{dt} = -\frac{2}{2!}K_3^{\mathrm{He}_2}n_{\mathrm{He}}^2 n_X - \frac{1}{2!}K_3^{\mathrm{He}X}n_{\mathrm{He}}^2 n_X, \tag{1}$$

where n_{He} and n_X designate the densities of helium and alkali-metal atoms, respectively; and $K_3^{\mathrm{He}X}$ and $K_3^{\mathrm{He}_2}$, the rates for three-body recombination $^4\mathrm{He}+{}^4\mathrm{He}+X\rightarrow{}^4\mathrm{He}+{}^4\mathrm{He}X$ and $^4\mathrm{He}_2+X$, respectively.

This paper is organized as follows. We explain our method and give all necessary formulas for calculating the three-body recombination rates in Sec. II. The results and discussion are presented in Sec. III. A summary of this work is given in Sec. IV. We use atomic units throughout except where explicitly stated otherwise.

II. METHOD

We solve the Schrödinger equation for three interacting atoms using a combination of the adiabatic hyperspherical representation [17,23,27,28] and the R-matrix method [31,32]. In the adiabatic hyperspherical representation, we calculate eigenfunctions and eigenvalues of the fixed-hyperradius Hamiltonian in order to construct a set of coupled radial equations. The R-matrix method is then used to extract the scattering matrix from these coupled equations. The method employed is largely the same as detailed in Refs. [17,23]. We thus give here only a brief outline and note any differences.

After separation of the center-of-mass motion, any three-particle system (in the absence of an external field) can be described by six coordinates. Three of these can be chosen as the Euler angles α, β, and γ that specify the orientation of the body-fixed frame relative to the space-fixed frame. The remaining three internal coordinates can be represented by a hyperradius R and two hyperangles θ and φ. To define these internal coordinates, we use a slightly modified version of the Smith-Whitten hyperspherical coordinates [17,23,29,30,33,34]. The hyperspherical coordinates $(R,\Omega) \equiv (R,\theta,\varphi,\alpha,\beta,\gamma)$ used in this work are defined in Ref. [23].

We rewrite the Schrödinger equation in terms of a rescaled wave function, which is related to the usual Schrödinger solution $\Psi_E(R,\Omega)$ by $\psi_E(R,\Omega)=R^{5/2}\Psi_E(R,\Omega)$. The volume element relevant to integrals over $|\psi_E(R,\Omega)|^2$ then becomes $2dR\sin 2\theta d\theta d\varphi d\alpha \sin\beta d\beta d\gamma$. The Schrödinger equation for three particles interacting through the potential $V(R,\theta,\varphi)$ now takes the form

$$\left[-\frac{1}{2\mu}\frac{\partial^2}{\partial R^2} + \frac{\Lambda^2}{2\mu R^2} + \frac{15}{8\mu R^2} + V(R,\theta,\varphi)\right]\psi_E(R,\Omega) = E\psi_E(R,\Omega), \tag{2}$$

where Λ^2 is the squared "grand angular-momentum operator" and its expression is given in Refs. [17,30,34]. The three-body reduced mass μ is given by

$$\mu^2 = \frac{m_1 m_2 m_3}{m_1+m_2+m_3}, \tag{3}$$

where m_i $(i=1,2,3)$ are the masses of particle i. In our convention, we shall designate the alkali-metal atom as particle 1 and the ^{4}He atoms as particles 2 and 3.

The interaction potential $V(R,\theta,\varphi)$ used in this work is expressed as a sum of three two-body terms,

$$V(R,\theta,\varphi) = v_{\mathrm{He}X}(r_{12}) + v_{\mathrm{HeHe}}(r_{23}) + v_{\mathrm{He}X}(r_{31}), \tag{4}$$

where r_{ij} are the interparticle distances. For the helium dimer potential $v_{\mathrm{HeHe}}(r)$, we use the representation of Jeziorska *et al.* [21], and for the helium–alkali-metal potentials $v_{\mathrm{He}X}(r)$ the KTTY representation of Kleinekathöfer *et al.* [26]. These potentials are plotted in Fig. 1. Our interaction potential in Eq. (4) includes neither retardation nor nonadditive three-body terms. Based on our experience in Ref. [23]. and the fact that helium atoms are not very polarizable, we do not expect the three-body term to contribute significantly. Retardation, however, may have a substantial effect on the rates [23]. To our knowledge, retardation corrections for HeX systems are not available. The $^4\mathrm{He}_2$ and $^4\mathrm{He}X$ bound-state energies $E_{vl}=E_{00}$ and the scattering lengths a calculated with these interaction potentials are summarized in Table I. These

TABLE I. $^4He_2$ and ^4HeX bound-state energy E_{00} (1 a.u. $=3.1577465\times10^8$ mK) and scattering lengths a calculated with the two-body potentials from [21,26].

System	E_{00} (a.u.)	E_{00} (mK)	a (a.u.)	a (Å)
$^4He_2$	-5.472×10^{-9}	−1.728	165.4	87.53
$^4He^7Li$	-1.780×10^{-8}	−5.622	92.29	48.84
$^4He^{23}Na$	-9.178×10^{-8}	−28.98	44.14	23.36
$^4He^{39}K$	-3.547×10^{-8}	−11.20	62.96	33.32
$^4He^{85}Rb$	-3.253×10^{-8}	−10.27	64.27	34.01
$^4He^{133}Cs$	-1.566×10^{-8}	−4.945	85.63	45.31

values agree well with the ones given by Refs. [21,26].

The first step that must be carried out is to solve the fixed-R adiabatic eigenvalue equation for a given symmetry J^Π, with Π the total parity, to determine the adiabatic eigenfunctions (or channel functions) and eigenvalues (or potential curves). The adiabatic eigenfunction expansion gives the wave function $\psi_E(R,\Omega)$ in terms of the complete orthonormal set of angular wave functions $\Phi_\nu(R;\Omega)$ and radial wave functions $F_{\nu E}(R)$

$$\psi_E(R,\Omega)=\sum_{\nu=0}^{\infty}F_{\nu E}(R)\Phi_\nu(R;\Omega). \tag{5}$$

The channel functions $\Phi_\nu(R;\Omega)$ and the potential curves $U_\nu(R)$ are eigenfunctions and eigenvalues of the five-dimensional partial differential equation

$$\left[\frac{\Lambda^2}{2\mu R^2}+\frac{15}{8\mu R^2}+V(R,\theta,\varphi)\right]\Phi_\nu(R;\Omega)=U_\nu(R)\Phi_\nu(R;\Omega), \tag{6}$$

whose solutions depend parametrically on R. Insertion of $\psi_E(R,\Omega)$ from Eq. (5) into the Schrödinger equation from Eq. (2) results in a set of coupled ordinary differential equations

$$\left[-\frac{1}{2\mu}\frac{d^2}{dR^2}+U_\nu(R)-\frac{1}{2\mu}Q_{\nu\nu}(R)\right]F_{\nu E}(R)-\frac{1}{2\mu}\sum_{\nu'\neq\nu}\left[2P_{\nu\nu'}(R)\frac{d}{dR}+Q_{\nu\nu'}(R)\right]F_{\nu' E}(R)=EF_{\nu E}(R). \tag{7}$$

The coupling elements $P_{\nu\nu'}(R)$ and $Q_{\nu\nu'}(R)$ involve partial first and second derivatives of the channel functions Φ_ν with respect to R, and are defined as follows:

$$P_{\nu\nu'}(R)=\left\langle\!\left\langle\Phi_\nu(R;\Omega)\left|\frac{\partial}{\partial R}\right|\Phi_{\nu'}(R;\Omega)\right\rangle\!\right\rangle, \tag{8}$$

and

$$Q_{\nu\nu'}(R)=\left\langle\!\left\langle\Phi_\nu(R;\Omega)\left|\frac{\partial^2}{\partial R^2}\right|\Phi_{\nu'}(R;\Omega)\right\rangle\!\right\rangle. \tag{9}$$

The double-bracket matrix element signifies that integrations are carried out only over the angular coordinates Ω.

In order to solve the adiabatic Eq. (6), we expand the channel function on Wigner D functions [17]

$$\Phi_\nu(R;\Omega)=\sum_K\phi_{K\nu}(R;\theta,\varphi)D^J_{KM}(\alpha,\beta,\gamma). \tag{10}$$

The quantum numbers K and M denote the projections of $\vec{J}$ onto the body-fixed and space-fixed z axes, respectively. K takes the values $J,J-2,\ldots,-(J-2),-J$ for the "party-favored" case, $\Pi=(-1)^J$, and $J-1,J-3,\ldots,-(J-3),-(J-1)$ for the "parity-unfavored" case, $\Pi=(-1)^{J+1}$, since K should be even for even parity and odd for odd parity [30]. The resulting complex coupled equations in θ and φ are solved by expanding $\phi_{K\nu}(R;\theta,\varphi)$ onto a direct product of fifth order basis splines [35] in θ and φ.

The identical particle symmetry of the two ^{4}He atoms can be built into the adiabatic equations via the boundary conditions. If we let particles 2 and 3 be the identical ones, then the permutation operation P_{23} corresponds to

$$\varphi\to2\pi-\varphi,\quad \alpha\to\alpha+\pi,\quad \beta\to\pi-\beta,\quad \gamma\to2\pi-\gamma,$$

$$D^J_{KM}\to(-1)^JD^J_{-KM}. \tag{11}$$

Consideration of this operation results in boundary conditions at $\varphi=0$,

$$(-1)^{J+K}\phi_{-K\nu}(R;\theta,0)=\phi_{K\nu}(R;\theta,0),$$

$$(-1)^{J+K+1}\left.\frac{\partial\phi_{-K\nu}}{\partial\varphi}\right|_{\varphi=0}=\left.\frac{\partial\phi_{K\nu}}{\partial\varphi}\right|_{\varphi=0}, \tag{12}$$

and at $\varphi=\pi$:

$$(-1)^J\phi_{-K\nu}(R;\theta,\pi)=\phi_{K\nu}(R;\theta,\pi),$$

$$(-1)^{J+1}\left.\frac{\partial\phi_{-K\nu}}{\partial\varphi}\right|_{\varphi=\pi}=\left.\frac{\partial\phi_{K\nu}}{\partial\varphi}\right|_{\varphi=\pi}. \tag{13}$$

With these, we need only consider the range $\varphi\in[0,\pi]$. Note that these boundary conditions differ from those described in Refs. [17,23], and the so-called postsymmetrization procedure used there is no longer necessary.

We generate the basis splines for θ from 100 mesh points, while we use 120 mesh points for φ. For small hyperradii R, a uniform mesh is employed; for large R, the mesh is designed so that it becomes dense around the two-body coalescence points at $(\theta,\varphi)=(\pi/2,\pi-2\arctan(m_2/\mu))$ and $(\pi/2,\pi)$ where the potential surface $V(R,\theta,\varphi)$ changes abruptly. This leads, for example, to a total basis size of 50 752 in the case of the 3^- symmetry. We autoparallelize the computer program in order to run it on multiple CPU cores. Typically, a calculation of the 15 lowest eigenvalues of the adiabatic Eq. (6) takes about 12 minutes of wall clock time using eight 1.6-GHz-Itanium2 CPU cores on an SGI Altix 4700 supercomputer.

In practice, we solve the adiabatic Eq. (6) for a set of about 200 radial grid points R_i up to $R \approx 2000$ a.u. in order to obtain the potential curves $U_\nu(R)$ and the coupling matrix elements $P_{\nu\nu'}(R)$ and $Q_{\nu\nu'}(R)$. For $R > 2000$ a.u. these are extrapolated using their known asymptotic forms. The other details of the numerical calculations are explained in Refs. [17,23].

III. RESULTS AND DISCUSSION

Since both the $^4He_2$ and ^{4}He–alkali-metal molecules have only a single $l=0$ bound state, three-body recombination is allowed only for the parity-favored cases, that is, $\Pi=(-1)^J$. In the following, we therefore limit ourselves to $J^\Pi = 0^+, 1^-, 2^+$, etc. For each of these cases, the lowest adiabatic potential curve $\nu=0$ corresponds asymptotically to a ^{4}He–alkali-metal molecule with one ^{4}He atom far away. Since this molecule has only $l=0$, the orbital angular momentum of the relative motion between the molecule and the atom should be $l_{2,31}=J$. This potential asymptotically behaves as

$$U_0(R) - \frac{1}{2\mu} Q_{00}(R) \to E_{00}^{\mathrm{He}X} + \frac{l_{2,31}(l_{2,31}+1)}{2\mu R^2}, \quad \text{for } R \to \infty, \tag{14}$$

where $E_{00}^{\mathrm{He}X}$ is the energy of the ^{4}He–alkali-metal molecule. The second lowest adiabatic potential curve $\nu=1$ corresponds asymptotically to two ^{4}He bound in a dimer with the alkali-metal atom far away, with the angular momentum of the relative motion $l_{1,23}=J$. Similarly, this potential asymptotically behaves as

$$U_1(R) - \frac{1}{2\mu} Q_{11}(R) \to E_{00}^{\mathrm{He}_2} + \frac{l_{1,23}(l_{1,23}+1)}{2\mu R^2}, \quad \text{for } R \to \infty, \tag{15}$$

where $E_{00}^{\mathrm{He}_2}$ is the energy of the ^{4}He dimer. All the higher channels $\nu=2,3,\ldots$ for each J^Π correspond to three-body continuum states i.e., all three atoms far away from each other as $R \to \infty$. Recall that in the adiabatic hyperspherical representation the three-body continuum is rigorously discretized since the adiabatic Hamiltonian depends only on the bounded hyperangles. These three-body continuum channel functions correlate asymptotically to the hyperspherical harmonics. Therefore, the corresponding potential curves behave as

$$U_\nu(R) \to \frac{\lambda(\lambda+4) + \frac{15}{4}}{2\mu R^2}, \quad \text{for } R \to \infty. \tag{16}$$

In principle, λ can take on any non-negative integer value, but their possible values are restricted by the requirements of permutation symmetry [36]. Figure 2 shows the potential curves $U_\nu(R)$ as functions of the hyperradius R for the ^{4}He-^{4}He-^{7}Li system with the $J^\Pi=0^+$ symmetry. Note that we have also calculated potential curves for the other ^{4}He-^{4}He–alkali-metal systems with several symmetries J^Π,

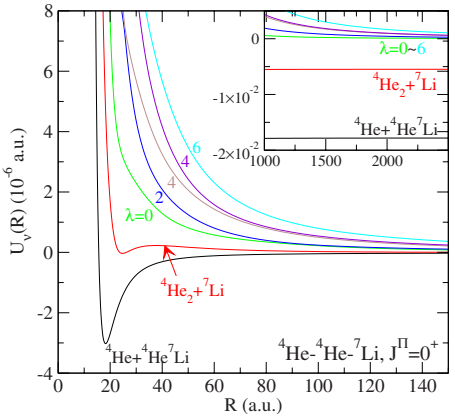

FIG. 2. (Color online) Adiabatic hyperspherical potential curves $U_\nu(R)$ for the ^{4}He-^{4}He-^{7}Li system with $J^\Pi=0^+$. The first and second lowest potential curves are the atom-molecule channels, and correspond asymptotically to ^{4}He+^{4}He^{7}Li and ^{4}He$_2$+^{7}Li, respectively. The higher channels represent the three-body continuum channels, and the values of λ indicate the asymptotic behavior of the potential curves, as given in Eq. (16). The inset shows the threshold region at large hyper-radii.

but they present similar features as the $J^\Pi=0^+$ ^{4}He-^{4}He-^{7}Li potential curves.

The scattering observables were obtained by solving the coupled Eqs. (7) using a combination of the finite element method (FEM) [32] and the R-matrix method [31,32]. Typically, about 12 adiabatic channels (thus $\nu_{\max}=11$) are used, and 10^4 elements, in each of which fifth order polynomials are used to expand the radial wave function, extend from $R=10$ to 5×10^5 a.u. The scattering S matrix is then extracted using the R-matrix method. Each energy took less than 1 minute of wall clock time using one 1.6 GHz Itanium2 processor on an SGI Altix 4700 supercomputer. We have checked the stability of the S matrix with respect to the final matching distance, number of FEM sectors, and the number of coupled channels, and have found our results accurate to three significant digits.

When the three-body system has two identical bosonic atoms, the total event rate constant for three-body recombination is expressed as

$$K_3 = \frac{k}{\mu}\sigma_3 = \sum_{J,\Pi} K_3^{J\Pi} = 2! \sum_{J,\Pi} \sum_{\nu=2}^{\nu_{\max}} \frac{32(2J+1)\pi^2}{\mu k^4} |S_{f\leftarrow\nu}^{J\Pi}|^2. \tag{17}$$

Here, σ_3 is the generalized three-body recombination cross section, $K_3^{J\Pi}$ the partial recombination rate corresponding to the J^Π symmetry, and $k=(2\mu E)^{1/2}$ the hyperradial wave number in the incident channel. $S_{f\leftarrow\nu}^{J\Pi}$ represents scattering from the initial three-body continuum channels ($\nu=2,\ldots,\nu_{\max}$) to the final atom-molecule channels ($\nu=f=0$ or 1) for the J^Π symmetry. The factor (2!) derives from the number of indistinguishable bosonic particles.

Figure 3(a) shows the partial rates $K_3^{J\Pi}$ for the $J^\Pi=0^+$, 1^-, 2^+, 3^-, 4^+, and 5^- symmetries and their total K_3 for three-body recombination ^{4}He+^{4}He+^{7}Li$\to$^{4}He+^{4}He^{7}Li as func-

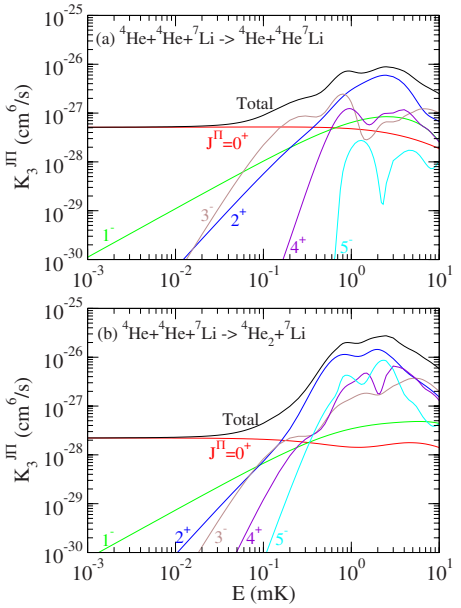

FIG. 3. (Color online) Partial rates $K_3^{J\Pi}$ and their total K_3 for the $J^\Pi=0^+$, 1^-, 2^+, 3^-, 4^+, and 5^- symmetries as functions of the collision energy E for the three-body recombination processes (a) ^{4}He $+^4$He$+^7$Li$\rightarrow^4$He$+^4$He^{7}Li and (b) ^{4}He$+^4$He$+^7$Li$\rightarrow^4$He$_2+^7$Li.

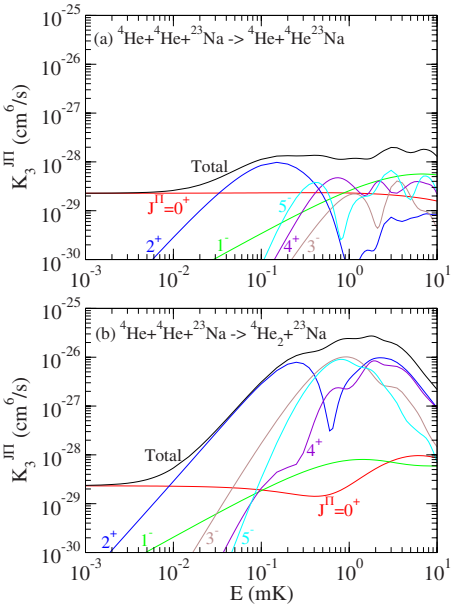

FIG. 4. (Color online) Partial rates $K_3^{J\Pi}$ and their total K_3 for the $J^\Pi=0^+$, 1^-, 2^+, 3^-, 4^+, and 5^- symmetries as functions of the collision energy E for the three-body recombination processes (a) ^{4}He $+^4$He$+^{23}$Na$\rightarrow^4$He$+^4$He^{23}Na and (b) ^{4}He$+^4$He$+^{23}$Na$\rightarrow^4$He$_2$ $+^{23}$Na.

tions of the collision energy E. At the lower collision energies, the partial recombination rates behave as $K_3^{J\Pi}\propto E^{\lambda_{\min}}$, where $\lambda_{\min}$ is the minimum value of λ in Eq. (16) allowed by permutation symmetry. For $J^\Pi=0^+$, 1^-, 2^+, 3^-, 4^+, and 5^- symmetries—that is, parity-favored cases—we have $\lambda_{\min}=0$, 1, 2, 3, 4, and 5 respectively, as predicted by a generalized Wigner threshold law [36]. This threshold behavior holds for any triatomic system, including two identical bosons, independent of the final recombination channel. For the whole energy range $10^{-3}\leq E\leq 10$ mK, the total of the partial recombination rates is converged to three digits with respect to the number of symmetries J^Π, and thus can be considered as the definitive total three-body recombination rate, unless the $J^\Pi=6^+$ or higher J states happen to be large. As a rule of thumb, the threshold regime can be characterized as energies smaller than the smallest energy scale which is typically a molecular binding energy. For each partial rate, the threshold regime is defined as the range of energies over which the generalized Wigner threshold law holds and can only really be determined *a posteriori*. This definition is sufficient theoretically, but only the total rate is physically observable, so the experimental threshold regime can be defined as the energy range over which the 0^+ rate dominates. The precise energy ranges from these two definitions need not coincide, especially when the 0^+ rate is suppressed. In our case, the smallest energy is the ^{4}He$_2$ binding energy of 1.7 mK. In Fig. 3(a), the partial recombination rates satisfy the generalized Wigner threshold law or the total rate is constant so that the threshold regime is attained for $E\lesssim 0.02-0.06$ mK—about two orders of magnitude smaller than the binding energy. This observation is in rough agreement with that for a purely helium collision system [23]. In the ultracold limit $E\rightarrow 0$, we obtain a total recombination rate of $K_3=5.12\times 10^{-28}$ cm^6/s. For the energies larger than about 0.1 mK, the partial rates with higher J become comparable to the 0^+ rate.

The partial rates $K_3^{J\Pi}$ and their total K_3 for recombination to the other available molecular channel, ^{4}He$+^4$He$+^7$Li $\rightarrow^4$He$_2+^7$Li, are presented in Fig. 3(b). At the lower collision energies, their behavior matches the above discussed threshold behavior. Unlike the ^{4}He$+^4$H^{7}Li channel, however, the 5^- rate contributes at the few percent level at higher energies. The convergence of the total rate at energies above roughly 1 mK is less certain. The 0^+ partial recombination rate oscillates slowly as a function of the collision energy, while small oscillations are observed in the $J\geq 2$ rates. In the ultracold limit $E\rightarrow 0$, we obtain a total recombination rate of $K_3=2.21\times 10^{-28}$ cm^6/s. This value is on the same order as (and slightly smaller than) the one for ^{4}He$+^4$He$+^7$Li $\rightarrow^4$He$+^4$He^{7}Li.

The results for the three-body collision ^{4}He$+^4$He$+^{23}$Na resulting in ^{4}He$+^4$He^{23}Na and ^{4}He$_2+^{23}$Na are presented in Figs. 4(a) and 4(b), respectively. We notice that the recombination rates to ^{4}He$+^4$He^{23}Na are significantly smaller than the ones to ^{4}He$+^4$He^{7}Li shown above. The recombination rate to ^{4}He$+^4$He^{23}Na is constant only for unusually low energies, that is, $E\lesssim 2$ μK, and the 2^+ partial recombination rate becomes rapidly comparable to the 0^+ rate at about 0.03 mK. However, the generalized Wigner threshold law is satisfied for collision energies one order of magnitude larger, so that, in this sense, the threshold regime corresponds to energies $E\lesssim 0.03$ mK. This is similar to the case of recombination to ^{4}He$_2+^{23}$Na in (b), for which the total recombination rate is constant only below about 1 μK and the 2^+ rate dominates over the 0^+ rate at about $E=0.01$ mK. In the ultracold limit $E\rightarrow 0$, the recombination rate for ^{4}He$+^4$He$+^{23}$Na$\rightarrow^4$He$+^4$He^{23}Na approaches $K_3=2.28\times 10^{-29}$ cm^6/s, while the rate for ^{4}He$+^4$He$+^{23}$Na

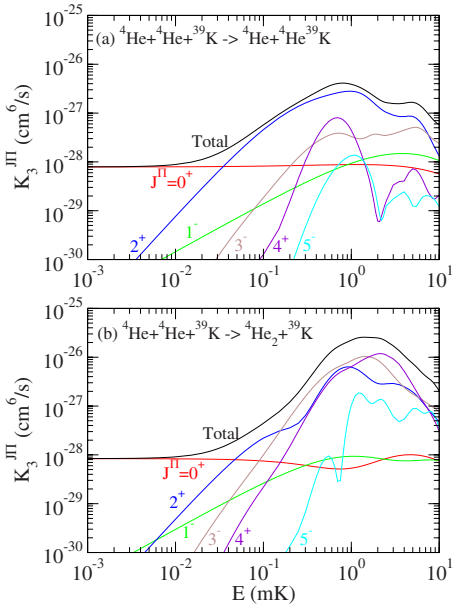

FIG. 5. (Color online) Partial rates $K_3^{J\Pi}$ and their total K_3 for the $J^\Pi=0^+$, 1^-, 2^+, 3^-, 4^+, and 5^- symmetries as functions of the collision energy E for the three-body recombination processes (a) ^{4}He $+^4$He$+^{39}$K$\rightarrow^4$He$+^4$He^{39}K and (b) ^{4}He$+^4$He$+^{39}$K$\rightarrow^4$He$_2+^{39}$K.

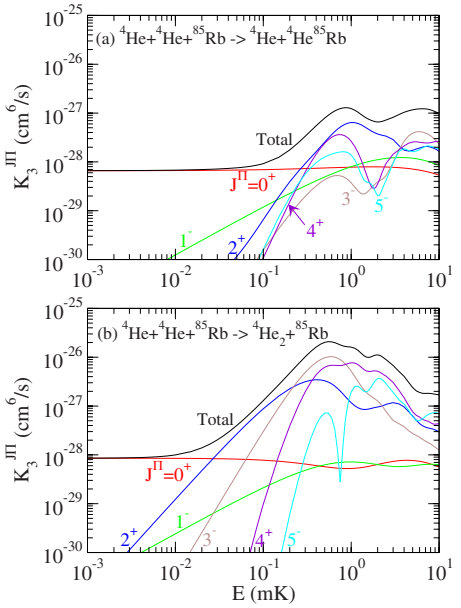

FIG. 6. (Color online) Partial rates $K_3^{J\Pi}$ and their total K_3 for the $J^\Pi=0^+$, 1^-, 2^+, 3^-, 4^+, and 5^- symmetries as functions of the collision energy E for the three-body recombination processes (a) ^{4}He $+^4$He$+^{85}$Rb$\rightarrow^4$He$+^4$He^{85}Rb and (b) ^{4}He$+^4$He$+^{85}$Rb$\rightarrow^4$He$_2$ $+^{85}$Rb.

$\rightarrow^4$He$_2+^4$He^{23}Na tends to a nearly identical value of K_3 $=2.32\times10^{-29}$ cm^6/s.

Figure 5 presents the three-body recombination rates for the ^{4}He-^{4}He-^{39}K system. In the same way, the results for three-body recombination rates for the ^{4}He-^{4}He-^{85}Rb and ^{4}He-^{4}He-^{133}Cs systems are presented respectively in Figs. 6 and 7. We find that all these partial recombination rates exhibit similar characteristics whichever alkali-metal species is involved. In the zero-energy limit $E\rightarrow0$, the total recombination rate K_3 tends to a constant value where the 0^+ partial rate dominates. At higher collision energies (that is, more than $10^{-2}-10^{-3}$ mK depending on the species and channel) the other symmetries—notably 2^+—become dominant over the 0^+ symmetry, while the contribution from the 1^- case is relatively weak. Several energy-dependent oscillations can be observed for the $J\geq2$ symmetries. The total three-body recombination rates at the zero-energy limit are summarized in Table II. Surprisingly, the rates for all systems lie within a relatively narrow range with the largest only about a factor of 20 more than the smallest. Further, we note that the threshold recombination rate for ^{4}He$+^4$He$+^4$He$\rightarrow^4$He$_2+^4$He is 9.93 $\times10^{-28}$ cm^6/s and for ^{4}He$+^4$He$+^3$He$\rightarrow^4$He$_2+^3$He is 9.83×10^{-27} cm^6/s [23]. Both of these are larger than any rate found here.

Given the progress in understanding the universal behavior of ultracold three-body scattering for weakly bound systems, it is tempting to try to analyze the present zero temperature results in relation to the universal expressions for K_3 [12,13,37]. Unfortunately, even though the HeX systems are weakly bound, these scattering lengths do not generally satisfy the universality requirement $a\gg r_0$ where r_0 is a characteristic length scale of the two-body potentials. For van der Waals potentials, one way to determine r_0 uses the C_6 coefficient and the two-body reduced mass μ_2: $r_0=(2\mu_2C_6)^{1/4}$.

We obtain $r_0\sim21-28$ a.u. for all of the HeX potentials. The systems closest to this limit are ^{4}He^{7}Li and ^{4}He^{133}Cs with $a/r_0\approx4$. It is known, however, that ^{4}He$_2$—with $a/r_0\approx16$—is just barely in the universal regime, making it unlikely that the present rates will show universal behavior. Ignoring the likely nonuniversality of our results and apply-

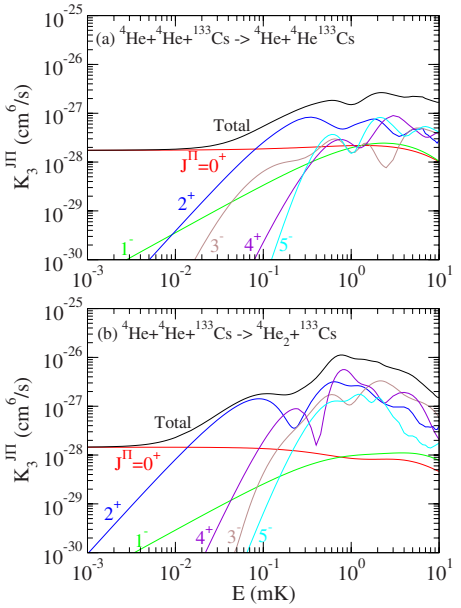

FIG. 7. (Color online) Partial rates $K_3^{J\Pi}$ and their total K_3 for the $J^\Pi=0^+$, 1^-, 2^+, 3^-, 4^+, and 5^- symmetries as functions of the collision energy E for the three-body recombination processes (a) ^{4}He $+^4$He$+^{133}$Cs$\rightarrow^4$He$+^4$He^{133}Cs and (b) ^{4}He$+^4$He$+^{133}$Cs$\rightarrow^4$He$_2$ $+^{133}$Cs.

TABLE II. Total three-body recombination rates $K_3(E\to 0)$ in the zero-energy limit for the ^{4}He-^{4}He–alkali-metal systems.

Initial channel	Final channel	$K_3(E\to 0)$ (cm^6/s)
^{4}He+^{4}He+^{7}Li	^{4}He+^{4}He^{7}Li	5.12×10^{-28}
	^{4}He$_2$+^{7}Li	2.21×10^{-28}
^{4}He+^{4}He+^{23}Na	^{4}He+^{4}He^{23}Na	2.28×10^{-29}
	^{4}He$_2$+^{23}Na	2.30×10^{-29}
^{4}He+^{4}He+^{39}K	^{4}He+^{4}He^{39}K	7.79×10^{-29}
	^{4}He$_2$+^{39}K	8.34×10^{-29}
^{4}He+^{4}He+^{85}Rb	^{4}He+^{4}He^{85}Rb	6.60×10^{-29}
	^{4}He$_2$+^{85}Rb	8.53×10^{-29}
^{4}He+^{4}He+^{133}Cs	^{4}He+^{4}He^{133}Cs	1.74×10^{-28}
	^{4}He$_2$+^{133}Cs	1.45×10^{-28}

ing the universal expectations anyway, we still face the question of which universal results to use. These systems can be treated as having three large, roughly equal scattering lengths in which case [8,9,12]

$$K_3 \propto a^4 \sin^2\left[s_0 \ln\frac{a}{r_0} + \Phi\right], \tag{18}$$

where s_0 is a constant that depends on the mass ratio, Φ is a short-range three-body phase that depends on the details of the potentials, and a is taken to be $(a_{\mathrm{HeHe}}a_{\mathrm{He}X}^2)^{1/3}$. These systems can also be treated as having two different scattering lengths satisfying $r_0 \ll a_{\mathrm{He}X} \ll a_{\mathrm{HeHe}}$. Under this condition, the recombination rates should be [37]

$$K_3^{\mathrm{He}_2} \propto a_{\mathrm{HeHe}}^4,$$

$$K_3^{\mathrm{He}X} \propto a_{\mathrm{He}X}^2 a_{\mathrm{HeHe}}^2 \sin^2\left[s_0 \ln\frac{a_{\mathrm{He}X}}{r_0} + \Phi\right]. \tag{19}$$

Finally, one might argue that only a_{HeHe} is large enough to be considered to be in the universal regime so that [38]

$$K_3^{\mathrm{HeHe}} \propto a_{\mathrm{HeHe}}^4,$$

$$K_3^{\mathrm{He}X} \propto a_{\mathrm{HeHe}}^2. \tag{20}$$

Although these expressions would seem to indicate similar rates for all X here, the missing proportionality constants depend on the species. Since none of these scenarios apply perfectly to the present systems due to the relatively small scattering lengths, we simply plot μK_3 versus $a_{\mathrm{He}X}/r_0$ in Fig. 8. We observe that the scattering length dependence $\mu K_3^{\mathrm{He}X} \propto (a_{\mathrm{He}X}/r_0)^4$ holds for recombination to the heteronuclear molecules. On the other hand, for a given alkali-metal species, the recombination rate to the ^{4}He dimer is roughly on the same order as the rate to ^{4}HeX molecules and satisfies the same dependence, that is $\mu K_3^{\mathrm{HeHe}} \propto (a_{\mathrm{He}X}/r_0)^4$. As stated above, though, these systems really do not lie in the universal regime, so the analysis represented by Eqs. (18)–(20) should not be expected to apply. The reason for such simple behavior in this nonuniversal regime is not known, but is an interesting question to explore.

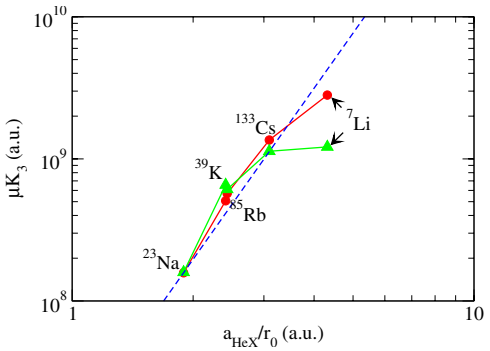

FIG. 8. (Color online) The filled circles show the mass-scaled recombination rates μK_3 for the processes ^{4}He+^{4}He+$X\to{}^4$He+^{4}HeX plotted against the ^{4}He-X scattering length $a_{\mathrm{He}X}/r_0$ (X = ^{7}Li, ^{23}Na, ^{39}K, ^{85}Rb, and ^{133}Cs). The filled triangles correspond to recombination to the ^{4}He dimer. The dashed line indicates the $(a_{\mathrm{He}X}/r_0)^4$ dependency of the mass-scaled rate.

IV. SUMMARY

In this work, we have studied three-body recombination in ^{4}He-^{4}He–alkali-metal collisions at cold temperatures. We have calculated the partial three-body recombination rates up to the $J=5$ symmetry. In the ultracold limit, the total recombination rate is constant and the $J^{\Pi}=0^+$ symmetry dominates, but at the collision energies larger than about 0.01 mK the higher J states become rapidly dominant. We have also found that the threshold regime is limited to unexpectedly low collision energies, that is, less than some tens of μK when we expected roughly 1 mK (the binding energy of ^{4}He$_2$). The rates K_3 for recombination ^{4}He+^{4}He+$X\to{}^4$He+^{4}HeX at threshold depend on the ^{4}He-X scattering length a and behave as $K_3\propto a^4$, whereas those for ^{4}He+^{4}He+$X\to{}^4$He$_2$+X are roughly on the same order as the ones to the heteronuclear molecules. At low energies, all these recombination rates are significantly smaller than the ones for ^{4}He+^{4}He+^{3,4}He$\to{}^4$He$_2$+^{3,4}He. As an extension of this work, the He+X+X collision processes are also interesting, but the large number of He+X_2 channels for alkali-metal atoms X currently pose technical difficulties.

ACKNOWLEDGMENT

B.D.E. acknowledges support from the US National Science Foundation.

[1] C. A. Stan, M. W. Zwierlein, C. H. Schunck, S. M. F. Raupach, and W. Ketterle, Phys. Rev. Lett. **93**, 143001 (2004).
[2] S. Inouye, J. Goldwin, M. L. Olsen, C. Ticknor, J. L. Bohn, and D. S. Jin, Phys. Rev. Lett. **93**, 183201 (2004).
[3] T. Weber, J. Herbig, M. Mark, H.-C. Nägerl, and R. Grimm, Phys. Rev. Lett. **91**, 123201 (2003).
[4] T. Kraemer *et al.*, Nature (London) **440**, 315 (2006).
[5] V. Efimov, Phys. Lett. **33B**, 563 (1970).
[6] V. Efimov, Nucl. Phys. A. **210**, 157 (1973).
[7] V. Efimov, Comments Nucl. Part. Phys. **19**, 271 (1990).
[8] E. Nielsen and J. H. Macek, Phys. Rev. Lett. **83**, 1566 (1999).
[9] B. D. Esry, C. H. Greene, and J. P. Burke, Phys. Rev. Lett. **83**, 1751 (1999).
[10] P. F. Bedaque, E. Braaten, and H.-W. Hammer, Phys. Rev. Lett. **85**, 908 (2000).
[11] E. Braaten and H.-W. Hammer, Phys. Rev. Lett. **87**, 160407 (2001).
[12] E. Braaten and H.-W. Hammer, Phys. Rep. **428**, 259 (2006).
[13] J. P. D'Incao and B. D. Esry, Phys. Rev. Lett. **94**, 213201 (2005).
[14] G. A. Parker, R. B. Walker, B. K. Kendrick, and R. T. Pack, J. Chem. Phys. **117**, 6083 (2002).
[15] R. A. Aziz and M. J. Slaman, J. Chem. Phys. **94**, 8047 (1991).
[16] R. A. Aziz, A. R. Janzen, and M. R. Moldover, Phys. Rev. Lett. **74**, 1586 (1995).
[17] H. Suno, B. D. Esry, C. H. Greene, and J. P. Burke, Phys. Rev. A **65**, 042725 (2002).
[18] J. R. Shepard, Phys. Rev. A **75**, 062713 (2007).
[19] E. Braaten, H. W. Hammer, D. Kang, and L. Platter, Phys. Rev. A **78**, 043605 (2008).
[20] E. A. Kolganova, A. K. Motovilov, and W. Sandhas, Phys. Part. Nucl. **40**, 206 (2009).
[21] M. Jeziorska, W. Cencek, B. Patkowski, B. Jeziorski, and K. Szalewicz, J. Chem. Phys. **127**, 124303 (2007).
[22] W. Cencek, M. Jeziorska, O. Akin-Ojo, and K. Szalewicz, J. Phys. Chem. A **111**, 11311 (2007).
[23] H. Suno and B. D. Esry, Phys. Rev. A **78**, 062701 (2008).
[24] P. Dehmer and L. Wharton, J. Chem. Phys. **57**, 4821 (1972).
[25] U. Kleinekathöfer, K. T. Tang, J. P. Toennies, and C. L. Yiu, Chem. Phys. Lett. **249**, 257 (1996).
[26] U. Kleinekathöfer, M. Lewerenz, and M. Mladenovic, Phys. Rev. Lett. **83**, 4717 (1999), for the cesium-helium KTTY potential in Table I, the parameters $A=1.224\,951$, $b_1=0.782\,095$, and $b_2=0.005\,131\,75$ must be adopted in order to correct a misprint (communication with U. Kleinekathöfer).
[27] B. D. Esry, C. D. Lin, and C. H. Greene, Phys. Rev. A **54**, 394 (1996).
[28] C. D. Lin, Phys. Rep. **257**, 1 (1995).
[29] B. R. Johnson, J. Chem. Phys. **73**, 5051 (1980).
[30] B. K. Kendrick, R. T. Pack, R. B. Walker, and E. F. Hayes, J. Chem. Phys. **110**, 6673 (1999).
[31] M. Aymar, C. H. Greene, and E. Luc-Koenig, Rev. Mod. Phys. **68**, 1015 (1996).
[32] J. P. Burke, Jr., Ph.D. thesis, University of Colorado, 1999.
[33] R. C. Whitten and F. T. Smith, J. Math. Phys. **9**, 1103 (1968).
[34] B. Lepetit, Z. Peng, and A. Kuppermann, Chem. Phys. Lett. **166**, 572 (1990).
[35] C. de Boor, *A Practical Guide to Splines* (Springer, New York, 1978).
[36] B. D. Esry, C. H. Greene, and H. Suno, Phys. Rev. A **65**, 010705(R) (2001).
[37] J. P. D'Incao and B. D. Esry, Phys. Rev. Lett. **103**, 083202 (2009).
[38] J. P. D'Incao and B. D. Esry, Phys. Rev. Lett. **100**, 163201 (2008).